ACS NANO

www.acsnano.org

ARTICLE

# Real-Time Capture and Visualization of Individual Viruses in Complex Media

Steven M. Scherr,[†] George G. Daaboul,[‡,§] Jacob Trueb,[†] Derin Sevenler,[⊥] Helen Fawcett,[†] Bennett Goldberg,[‡,⊥,∥] John H. Connor,[⊥,¶,#] and M. Selim Ünlü*[,‡,⊥,∥,#]

[†]Mechanical Engineering Department, [‡]Electrical and Computer Engineering Department, [⊥]Biomedical Engineering Department, and [∥]Physics Department, Boston University, Boston, Massachusetts 02215, United States

[§]nanoView Diagnostics Inc., Boston, Massachusetts 02215, United States

[¶]Microbiology Department, Boston University School of Medicine, Boston, Massachusetts 02118, United States

Supporting Information

**ABSTRACT:** **Label-free imaging of individual viruses and nanoparticles directly in complex solutions is important for virology research and biosensing applications. A successful visualization technique should be rapid, sensitive, and inexpensive, while needing minimal sample preparation or user expertise. Current approaches typically require fluorescent labeling or the use of an electron microscope, which are expensive and time-consuming to use. We have developed an imaging technique for real-time, sensitive, and label-free visualization of viruses and nanoparticles directly in complex solutions such as serum. By combining the advantages of a single-particle reflectance imaging sensor, with microfluidics, we perform real-time digital detection of individual 100 nm vesicular stomatitis viruses as they bind to an antibody microarray. Using this approach, we have shown capture and visualization of a recombinant vesicular stomatitis virus Ebola model (rVSV-ZEBOV) at 100 PFU/mL in undiluted fetal bovine serum in less than 30 min.**

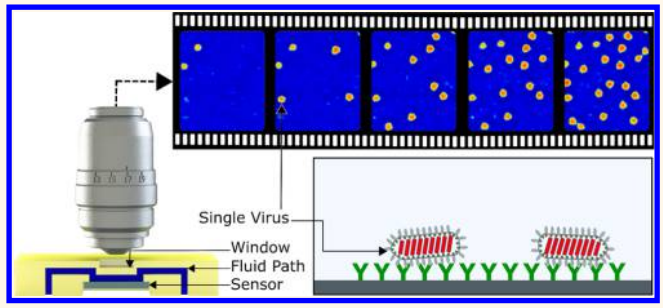


**KEYWORDS:** *single virus, interferometry, biosensor, Ebola, label-free*

Direct optical detection and visualization of viruses in liquid is very challenging because they are small and have low dielectric contrast with the surrounding medium and thus weakly interact with light.[1,2] Current approaches for imaging viruses in solution use indirect approaches such as purification followed by fluorescent labeling or genetic modification of viral proteins.[3,4] These approaches provide important virus-tracking abilities but offer little information about the virus particle itself. Direct imaging of viruses has historically been accomplished through electron microscopy (EM). EM provides impressive resolution but requires significant preparation, expertise, and often sample desiccation and degradation.[5]

Several other techniques have been developed for virus and nanoparticle visualization that are based on light scattering and in-liquid transmission electron microscopy in addition to nonimaging approaches such as nanopore ionic current that can be used to gain information about viruses and nanoparticles.[6−9] Some of these techniques have proven to be very useful in various research fields such as virology and vaccine development, but each has different capabilities and merits related to sample throughput, cost, user expertise, and specificity.[10,11] A technique that is capable of combining the benefits of these systems would be of high utility across a variety of fields.

Various novel optical sensor systems have been developed in an attempt to meet these needs, such as surface plasmon resonance,[12] high-Q resonant structures,[13] and diffractive optics.[14] There have also been other interferometry-based techniques for detecting viruses, such as those using a young interferometer[15] and dark-field interferometry.[16] Each of these optical sensors has unique benefits, but none has truly filled the gap to provide robust, direct, and chemically specific high-throughput single-particle visualization in a complex sample. There remains a need for a bridging technology between traditional wide-field microscopy and high-resolution electron microscopy.

Here, we describe the development of an imaging approach we have named single-particle interferometric imaging sensing (SP-IRIS). SP-IRIS enables visualization and counting of viruses in solution without the need for virus labeling. This allows for the study of unmodified viruses using visible light

Received: December 16, 2015
Accepted: January 13, 2016
Published: January 13, 2016




DOI: 10.1021/acsnano.5b07948
ACS Nano 2016, 10, 2827−2833

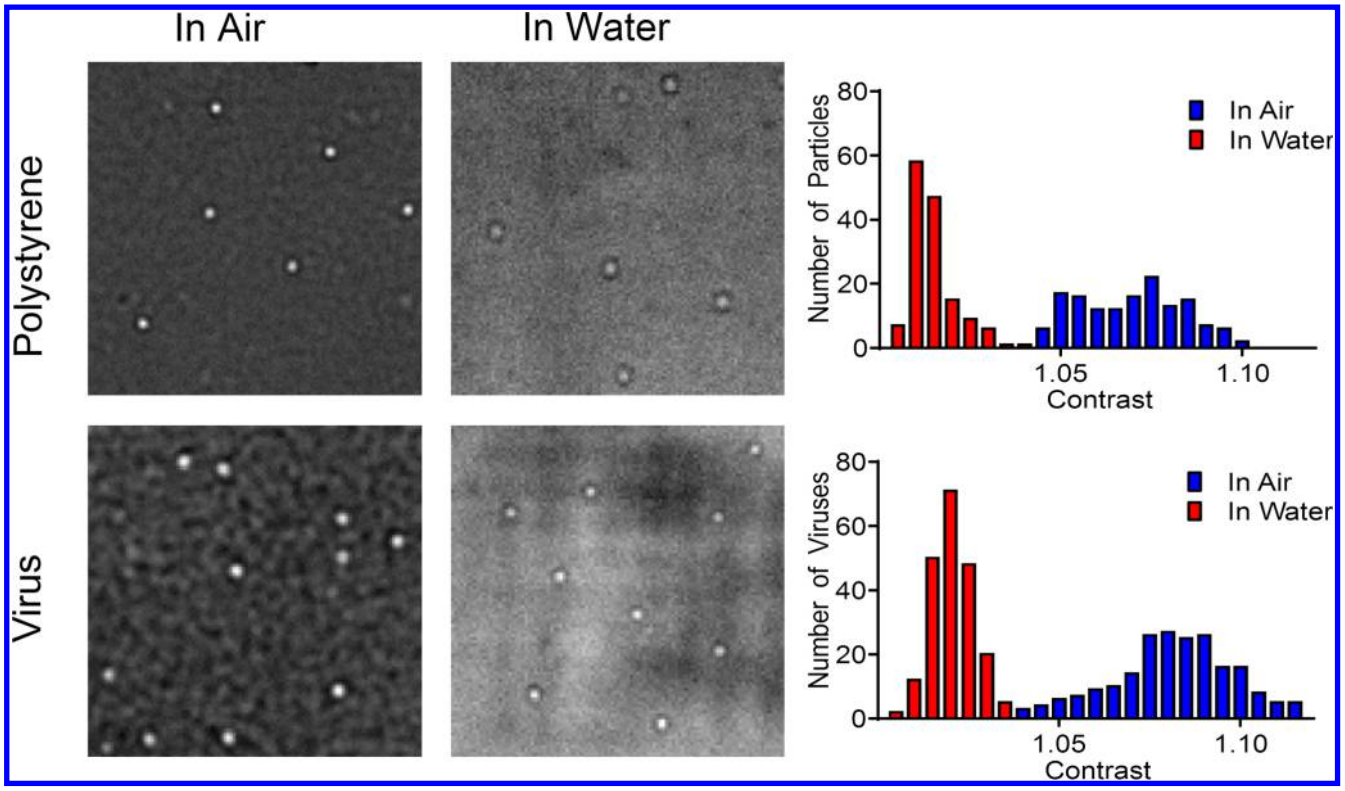


**Figure 1. Images of unlabeled 104 nm polystyrene beads imaged in air and water as well as native unlabeled virus particles imaged in air and water. Each bright dot is the image of a single nanoparticle or virus. A contrast histogram shows the contrast of the particles compared to the local background of the image in both air and water.**

microscopy. Our approach allows individual virus quantification in end point assays as well as dynamic detection as they are being captured on the sensor surface in solutions ranging from buffer to serum. SP-IRIS offers an additional imaging benefit for investigating nanoparticles in general and virus biology specifically by enabling the rapid counting of virus populations and evaluation of size distributions within complex media such as serum, an analysis not possible using traditional light microscopy and prohibitively time-consuming by EM. The ability to quantify and obtain size and shape information on a large number of individual viruses captured on a sensor surface has significant utility for understanding basic virus/antibody and virus/receptor interactions. In addition, this approach has the potential to serve as a highly sensitive rapid detection platform of pathogens with minimal sample preparation. We show that SP-IRIS can identify virus particles captured on the sensor surface from solutions containing only a few tens of replication-competent viruses.

## RESULTS AND DISCUSSION

**Sensing Platform for Imaging of Unlabeled Low-Contrast Nanoparticles and Native Virus Particles in Liquid.** To visualize nanoparticles, a silicon substrate with a thermally grown oxide layer was used to enhance the interferometric signal from individual particles.[17,18] Particles captured on the sensor surface had a much stronger signal than particles in solution at an arbitrary distance from the surface due to the interference enhancement optimized by the silicone oxide spacer. This enhancement causes particles on the surface to become visible, while particles floating in solution do not hinder imaging. To understand how changing the medium affected the signal produced by the interaction of light with nanoparticles, the classical theory of induced dipoles on a nonabsorbing particle was used. The quasi-static theory relates the strength of the induced dipole to the polarizability of the particle

$$\alpha = 4\pi\varepsilon_0 r^3 \frac{\varepsilon_p - \varepsilon_m}{\varepsilon_p + 2\varepsilon_m}$$

where $r$ is the particle radius, $\varepsilon_p$ is the particle permittivity, and $\varepsilon_m$ is the surrounding medium permittivity.[1] In most nonmagnetic materials, the permittivity can be approximated by the square of the refractive index. By increasing the refractive index of the medium from $n = 1$ in air to $n = 1.33$ in water, the index contrast of the particle to the surrounding medium is reduced, resulting in a weaker induced dipole. Therefore, we expect about a 3-fold reduction in signal going from dry to in-liquid imaging. A multifaceted approach was required to overcome the difficulties imposed by the reduced contrast. We optimized the oxide thickness for in-liquid imaging, utilized a cover-glass-corrected objective to reduce optical aberrations, and used image processing techniques such as illumination normalization and background subtraction.

**Capture and Imaging of Unlabeled Nanoparticles and Native Virus Particles in Liquid.** The SP-IRIS technique has been shown to be effective at imaging individual viruses and nanoparticles on the dry sensor surface with high sensitivity. Because this approach required both washing and drying steps prior to particle imaging, we investigated whether we could adapt SP-IRIS in a fashion that would allow imaging of nanoparticles and viruses in a liquid environment.

In order to validate the ability of SP-IRIS to image viruses in solution, polystyrene beads were used as a model because they have a size and refractive index similar to those of many viruses.



DOI: 10.1021/acsnano.5b07948
ACS Nano 2016, 10, 2827−2833

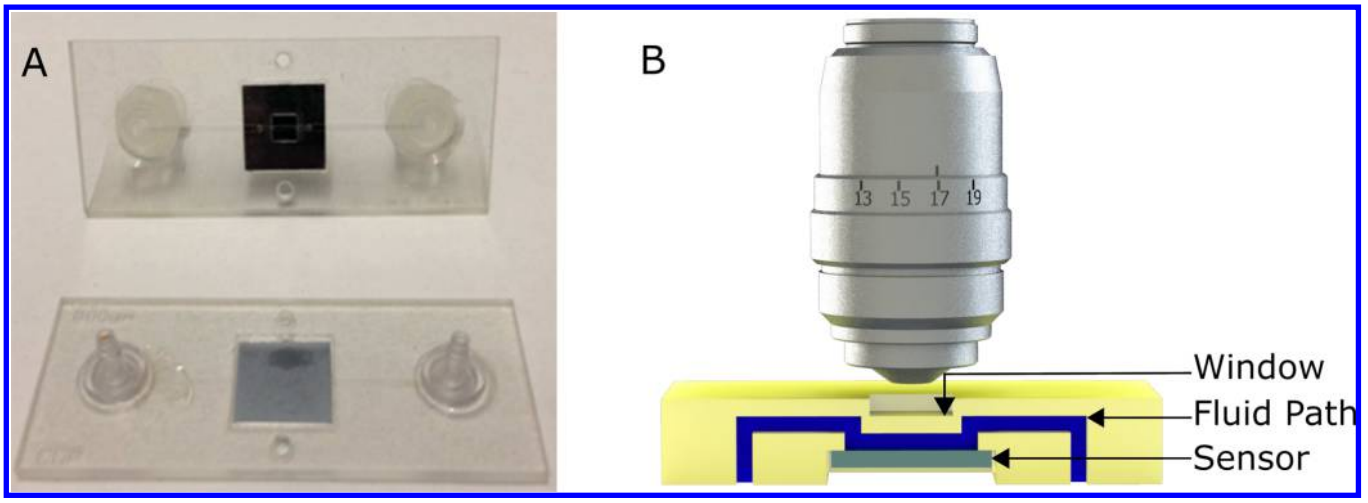


**Figure 2. (A) Pcture of the first generation polymeric cartridge used for virus and nanoparticle imaging. (B) Cross section model which demonstrates the fluidic path (in blue), the sensor (in gray) and the chip and window (in yellow) not to scale.**

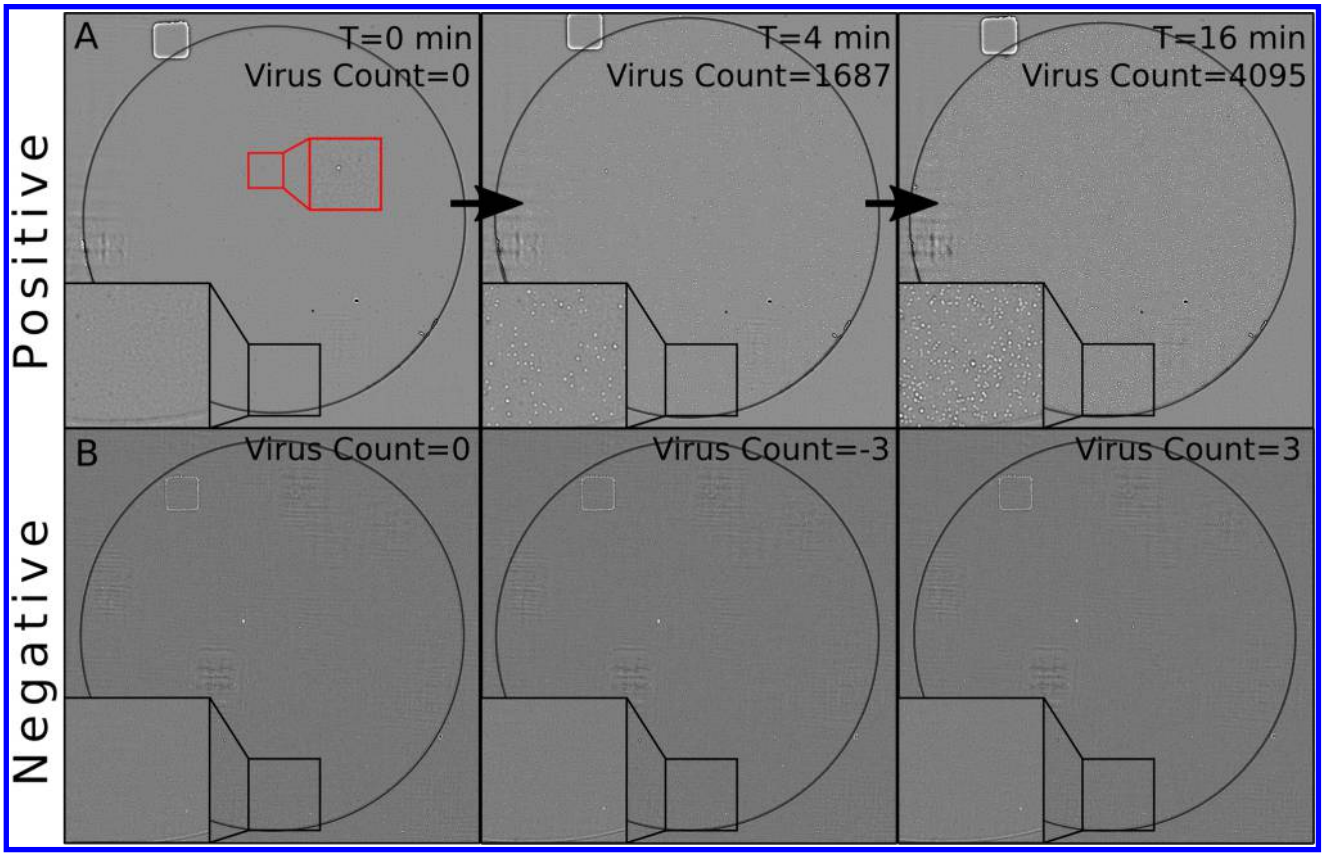


**Figure 3. (A) Anti-Ebola antibody spot imaged before the sample incubation begins and images taken at 4 and 16 min, showing the accumulation of viruses on the surface. (B) Negative control antibody imaged at the same time points that does not capture rVSV-ZEBOV. The black insets show a close-up view of the spot and the individual viruses. The red inset in the first time point ($T$ = 0) shows debris that is present at the beginning of the experiment. These are not counted as viruses because they are present before the incubation begins. The antibody spots are circled to improve visibility.**

Polystyrene beads were spun onto a substrate and imaged in air and under a window containing deionized water to investigate the effect on the signal. Figure 1 shows the signal produced by a 104 nm polystyrene bead bound to the IRIS substrate in a dry environment with a mean contrast 6.7% greater the local background. The signal produced by the same particles when imaged label-free in liquid was weaker but still clearly distinguishable from the background with a mean contrast of 1.7% greater than the local background. This shows that there is a significantly reduced contrast of nanoparticles when imaged in a liquid environment, but nevertheless, dielectric nanoparticles remain clearly detectable in solution.

Encouraged by imaging polystyrene beads in solution, we investigated the effectiveness of this technique for visualization of bona fide virus particles. To determine whether viruses in solution could be captured and visualized, we printed anti-



DOI: 10.1021/acsnano.5b07948
*ACS Nano* 2016, 10, 2827−2833

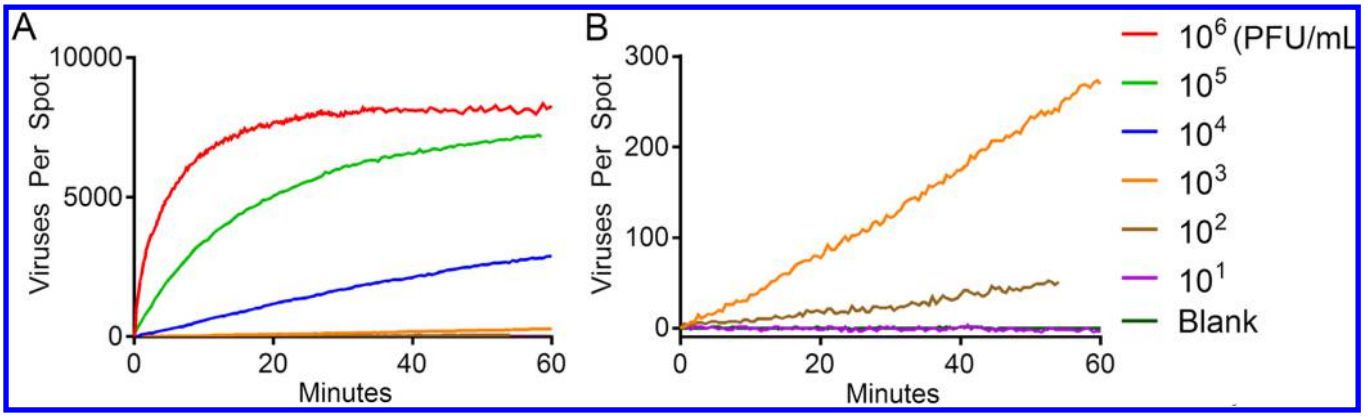


**Figure 4. (A) Accumulation of viruses being imaged on the sensor for a serial dilution ranging from 1 × $10^6$ PFU/mL down to a blank sample. The high concentration samples show a very rapid accumulation of viruses followed by a saturation of the sensors. (B) Lower concentrations expanded, showing a linear accumulation of viruses and a limit of detection of 100 PFU/mL in less than 60 min.**

Ebola antibody capture probes (13F6) on the surface of the sensor. The sensor surface was first coated in an antifouling polymer which was designed to enhance adsorption of proteins and enable consistent antibody microarrays.[19] A protein microarray consisting of ~150 $\mu$m diameter spots of an antibody that specifically recognizes the surface glycoprotein of Ebola virus was deposited on the layered sensor surface along with separate control spots of an antibody that does not recognize the Ebola virus glycoprotein.

To investigate whether virus particles could be captured by these arrays and individually visualized, a recombinant vesicular stomatitis virus that expresses the surface glycoproteins of the Zaire strain Ebola (rVSV-ZEBOV) was used as a model virus.[20,21] Dilutions of the rVSV-ZEBOV viruses were incubated with the antibody microarray (for some amount of time). The signal of the captured viruses imaged in air (dry) appeared very similar to the polystyrene bead with a mean contrast 8.0% greater than the local background. When the same microarray was used to image the virus on the surface of the chip while in solution (PBS), the signal again appeared similar to that of polystyrene particle imaged label-free, showing a mean contrast of 2.1% greater than the local background. As expected, virus particles show a similar reduction in contrast to polystyrene beads. This approach provides sufficient information for robust label-free, wide-field visualization of viruses and nanoparticles in solution.

**Real-Time Detection of Individual Viruses.** The ability to directly image nanoparticles and viruses in a liquid environment raised the possibility that we could observe the capture of particles as these events occurred in real-time. Real-time visualization implies the ability to distinguish between individual binding events temporally. It should be noted that a high temporal resolution is not needed for low-concentration samples that produce infrequent binding events. Due to our interest in low concentrations, a 30 s time resolution was deemed sufficient for this study. The temporal resolution for imaging a single sensor is limited primarily by the hardware, and acquisition at over 1000 fps can be achieved by simply using a different camera. This would allow the ability to distinguish individual events temporally at even the highest concentrations tested.

To test this modality, a microfluidic flow cell (shown in Figure 2A) was designed to allow imaging of the virus capture during sample incubation. Figure 2B shows the fluid path of this flow cell in blue. The fluid must move up and over the edge of the embedded sensor then down and across the sensor surface before exiting the cartridge. External fluidic connections on the chip allowed fluid to be driven across the chip sensor surface by a syringe pump before exiting to a waste reservoir.

Using this microfluidic chamber, a solution of PBS containing virus was directed through the fluid channel and across the IRIS detection chip containing specific and nonspecific antibodies. Images of the IRIS chip surface were recorded every 30 s. Following image acquisition, individual particles were counted using custom particle detection software. In this software, pre-existing debris found in the initial image before incubation begins is subtracted from subsequent measurements. Viruses that were captured on the sensor surface appeared as bright dots, as seen in Figure 3A (compare insets at $t$ = 0 and $t$ = 4), and the number of bound particles (virus count) continued to increase over the 16 min time course shown here. The red inset in Figure 3A shows an example of a particle that would not be counted as a virus because it was present before the experiment began. Figure 3B shows the images obtained from a negative control antibody for wild-type VSV that should not show capture of rVSV-ZEBOV. The antibodies show very good selectivity and nearly no cross-reactivity demonstrated by the lack of virus capture in Figure 3B. The negative virus count in Figure 3B can occur due to nanoparticle debris or protein aggregates on the antibody spot washing away, as well as imperfect focus and the difficulty in repeatedly detecting very small particles. Additionally, particles of different size have different contrast, which allows size discrimination and filtering to restrict particle counting to those signals conforming to the expected size of the virus particle. Analysis using this program showed the capture of virus particles beginning at $T$ = 0.5 min, and that there were an increasing number of particles detected over the time course of the experiment on the anti-Ebola antibody (from $T$ = 0 to $T$ = 16 min) in Figure 3A but not on the negative control antibody (Figure 3B). All data shown here were analyzed after the assay was completed. However, the software has be modified to allow the algorithm to operate in real-time during the assay.

**Virus Detection Sensitivity Directly in Buffer Solution.** Having established that virus particles could be directly detected as they were captured onto an IRIS chip, we then determined the performance and specificity of our sensor system. To do this, we conducted dilution experiments for rVSV-ZEBOV spiked in PBS with 1% BSA and measured the limit of detection. To detect viruses as they bind to the surface,


DOI: 10.1021/acsnano.5b07948
ACS Nano 2016, 10, 2827–2833

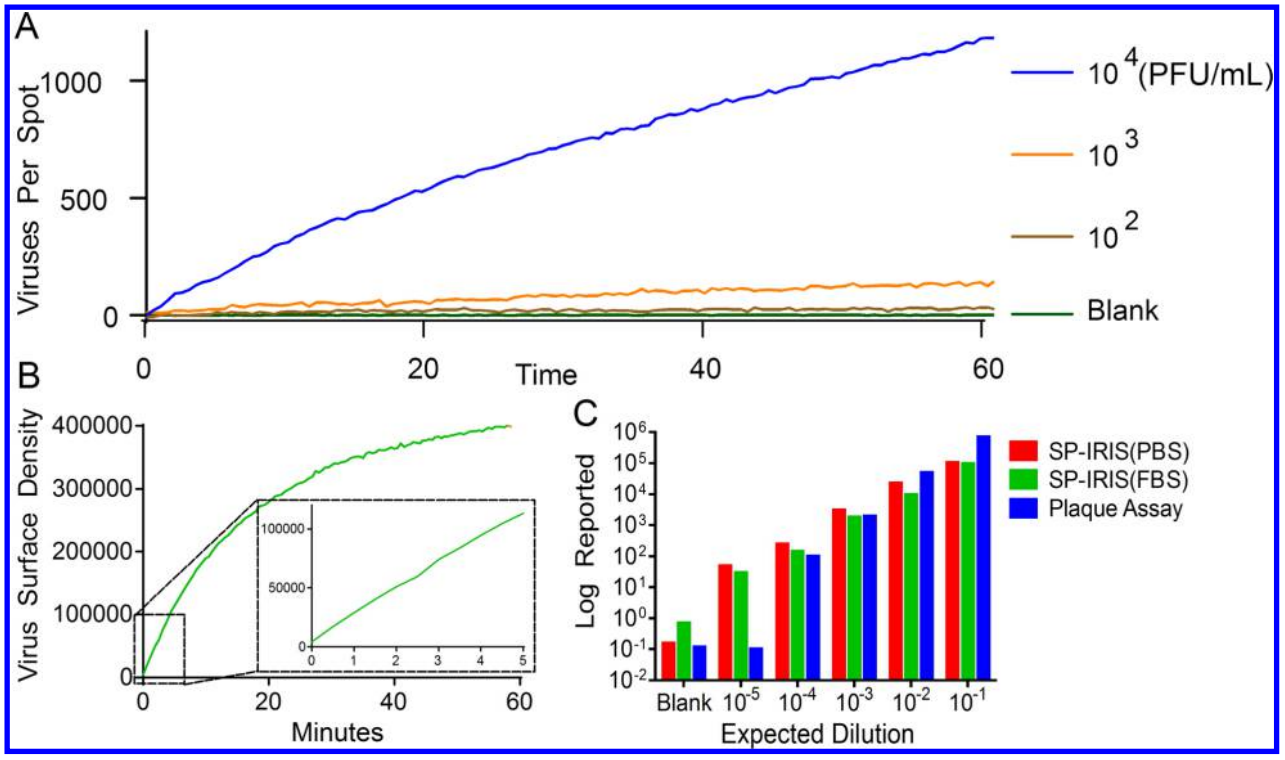


**Figure 5. (A) Accumulation of rVSV-ZEBOV viruses for a serial dilution. Images were taken directly in 100% FBS without washing or labeling. (B) Linear binding region in the first 5 min of the binding curve for a high concentration of virus plotted as viruses captured per mm$^2$. (C) Binding rate in units of particles/mm$^2$/min for rVSV-ZEBOV in PBS, and FBS shows a linear response to virus concentration. This is shown along with the plaque assay on the same plot, which uses units of PFU/mL to show that this may be used as a means of quantifying viral concentration. Plaque assay zero values are reported as $10^{-1}$.**

a single ~150 $\mu$m antibody spot within the microarray was imaged at discrete time intervals to create a motion picture of viruses binding to the surface. These images were then analyzed to create a curve of the number of viruses bound to the surface as a function of time. The number of viruses captured on a spot was reported by taking the virus density detected and normalizing to the area of a 150 $\mu$m diameter spot.

For our sensitivity experiments, six different dilutions were made from the stock virus solution (~$10^7$ PFU/mL) and samples ranging from a 10-fold dilution (~$10^6$ PFU/mL) to a $10^6$ fold dilution (~10 PFU/mL), including a blank sample containing no virus. A portion of each dilution was passed over an IRIS detector chip within the flow cartridge described above. A second portion of each dilution was used to determine virus concentration *via* plaque assay. The incubation of the virus solution in the microfluidic housing consisted of flowing at 1 $\mu$L/min for 1 h, recording images every 30 s.

Figure 4A shows the full dilution curve in PBS with 1% BSA. The highest concentration tested was $1 \times 10^6$ PFU/mL, which shows rapid accumulation of viruses binding on the surface. This showed a short period of linear virus accumulation, followed by saturation after about 30 min. Saturation levels are affected by the particle detection software's inability to discriminate between closely bound particles (further discussed in the Methods section). The saturation level shown here is an optical saturation and not a chemical equilibrium. Noise in the signal, such as a negative shift, is primarily due to the particle detection software imperfectly detecting or filtering particles that were found in previous images. To a lesser extent, some previously bound virus particles do unbind. However, avidity effects of multiple binding interactions are expected on a single virus, which should greatly reduce unbinding.

Lower concentration samples showed a slower rate of virus accumulation but appeared to approach similar saturation values. This saturation results from the inability to differentiate individual particles that are bound too closely together on the sensor surface. Despite this saturation, highly concentrated samples can still be differentiated based on the initial binding rate. Figure 4B shows that detection was clearly visible down to very low concentrations. This shows concentrations of $1 \times 10^3$ PFU/mL and below. As can be seen from Figure 4B, even at 100 PFU/mL, the signal is clearly differentiable from the blank sample in less than 30 min. At such low concentrations, the accumulation of virus remains linear for the duration of the experiment. The lowest concentration tested was 10 PFU/mL and was indistinguishable from a blank sample of PBS that contained no virus. The inability to detect viruses at 10 PFU/mL and below is due to the fact that virions must be captured on the surface to be counted. Some viruses in the sample will flow through the channel and not come into contact with the antibody-coated surface and thus are not captured and detected. The fact that particles in solution far from the sensor surface are not visualized allows us to image through complex samples without significant obstruction.

Previous work has shown the limit of detection of SP-IRIS in air to be $5 \times 10^3$ PFU/mL.[22] This work improves upon previous results by a 50-fold increase in sensitivity in half the time. In addition, this work removes all washing and drying steps by imaging directly in the liquid environment instead of in air, greatly reducing the complexity of the assay. This work shows rapid detection as well as a biologically relevant limit of


DOI: 10.1021/acsnano.5b07948
ACS Nano 2016, 10, 2827–2833

detection. The kinetics of capture showed a strong concentration dependence and broad dynamic range.

**Virus Detection and Quantification Directly in Complex Solutions.** To further explore the applicability of our technique, we explored the ability to image viruses directly in complex media such as serum. The ability to image viruses directly in serum would eliminate the need for most sample preparation approaches as is standard for current methods of virus imaging. To determine the capability and specificity of SP-IRIS in direct label-free detection of viruses in 100% fetal bovine serum, a second dilution curve was done using rVSV-ZEBOV. The same protocol was followed as in the dilution curve performed in PBS with 1% BSA that was previously described.

Figure 5A shows the results from these experiments, which track very closely with the dilution curve in PBS. The highest concentration shows rapid accumulation of virus on the surface with a similar decrease in binding as a large amount of virus accumulates. The higher concentrations (not shown) demonstrate a similar saturation as the previous experiment. More importantly, the lower concentrations show a linear accumulation rate for the entirety of the experiment. In addition, the limit of detection of rVSV-ZEBOV in serum is 100 PFU/mL, which is the same limit determined for PBS. This demonstrates that our technique is capable of imaging virus particles captured on the surface of an IRIS chip while the virus resides in complex media. Further, although the serum contains a number of its own nanoparticles and proteins and is not optically clear, virus imaging was possible without a significant reduction in signal.

These curves indicate that each concentration shows a distinct accumulation rate which can be used to differentiate between sample concentrations. In order to show that the sensor has a concentration-dependent signal, a linear curve was fit to the time-resolved virus count for each concentration. For the high concentrations that demonstrated nonlinear behavior, the curve was fit using just the first few minutes of the experiment, as shown in Figure 5B. Figure 5C reports this binding rate in viruses bound per minute per $mm^2$ plotted *versus* the log dilution of the stock virus sample. The dilutions were also tested using plaque assay and reported in PFU/mL. The binding rate for this sensor shows a linear response over a range of 4 orders of magnitude in both PBS and 100% FBS and good correlation to the expected concentration. This shows that SP-IRIS can provide semiquantitative results over a large dynamic range while maintaining very high sensitivity.

## CONCLUSIONS

A direct, rapid virus quantification technique that correlates well to standard virus quantification methods would be useful across a range of applications from virology research to diagnostic applications. We have demonstrated a specific label-free virus detection technique that allows visualization of individual viruses as they bind to a surface directly in a complex media. Of particular importance is the ability of this approach to visualize particles in solution with minimal sample preparation. This technique will help to bridge the gap between conventional optical microscopy and electron microscopy by allowing label-free optical detection of individual viruses within native fluids. By detecting individual viruses, this approach represents the ultimate limit of detection sensitivity. To demonstrate the capability of this technique for virus analysis, we showed real-time label-free detection of an Ebola model at 100 PFU/mL in less than 30 min. This technique was implemented directly in serum without the need for additional sample purification or amplification in a low-cost polymer-based cartridge. When compared to other techniques such as ELISA or PCR, this method requires no fluorescent labeling and minimal user expertise. In solution, SP-IRIS measurements demonstrate a new platform for virology research and pathogen detection that is capable of time-resolved, label-free visualization of individual viruses.

## METHODS

**SP-IRIS Instrumentation.** SP-IRIS imaging platform is a wide-field microscope that utilizes a 530 nm green LED for sample illumination in a Koehler illumination configuration.[17] The sample is imaged with either a 50× 0.8 NA Nikon objective for dry samples or a 40× 0.9 NA Nikon objective for samples in liquid onto a CCD camera (Retiga 4000R, Qimaging). The instrument averaged 10 frames per image, at an exposure of 6 ms per frame, recorded at 4 fps. The total integration time was 60 ms per image. The platform images the intensity of the particle signal compared to the nearby background intensity. The signal is based upon the interference between the scattered field from the particle of interest and the reference field reflected off a layered sensor surface. Thus, the optical system parameters are optimized in accordance with the optical properties of the target particles and the sensor structure. SP-IRIS utilizes custom particle detection software developed in Matlab to identify particle-associated local intensity maxima and applies filters to remove nondiffraction limited peaks.

**Particle Detection Software.** Virus particle detection is performed on the saved images using a custom program developed in Matlab. The software uses a modified scale invariant feature transform to detect particles.[18,23] This technique detects regions of light or dark contrast compared to the local background. Particle contrast is then defined as the peak pixel intensity compared to the local neighboring pixels. Particles are also scored by comparing the point spread function of the particle to a Gaussian template. This allows filtering of potential particles based on both contrast and correlation. This process is described in further detail in the Supporting Information.

**Sensor Preparation.** The substrates used for the sensor were purchased from Silicon Valley Microelectronics. The substrates were polished silicon with thermally grown oxide on top. The thickness of the oxide layer was adjusted to optimize the signal (contrast) enabling highly sensitive detection and counting of nanoscale particles. An oxide thickness of 100 nm was used for imaging in air, while 30 nm thickness was used for imaging in liquid. The sensor surface was coated in an antifouling copolymer with NHS groups to promote binding antibody probes. Anti-Ebola glycoprotein antibody (13F6) was provided by Larry Seitlin at Mapp Biopharmaceutical, San Diego, for the capture of rVSV-ZEBOV. For a negative control antibody, an antibody against native VSV was used (8G5). A Scienion S3 SciFlexArrayer was used to create an array of antibody probes. The sensors were left for 24 h to allow time for the antibodies to immobilize on the surface. Any unbound antibody was then washed with 1× PBST (0.1% Tween-20) followed by Nanopure-filtered deionized water and dried under a nitrogen gun. Arrayed sensors were stored refrigerated at 4 °C and used within 7 days. Mouse monoclonal antibody against VSV glycoprotein was produced from hybridoma cells for use as a negative control antibody. Mouse monoclonal against Ebola-Zaire was provided to us from the United States Army Medical Research Institute of Infectious Diseases.

**Virus Incubation in Buffer and Serum.** Virus stock was provided in cell media solution. All limit of detection experiments were conducted from a single stock solution serially diluted. For dilution experiments, all virus titers were confirmed using plaque assay. All experiments conducted in buffer used 1× PBS with 1 mg/mL bovine serum albumin added. Fetal bovine serum was purchased from ATCC (#30-2020). All experiments were conducted in a cartridge with fluid controlled by a Harvard Apparatus PhD 2000 syringe pump. Just prior


DOI: 10.1021/acsnano.5b07948
*ACS Nano* 2016, 10, 2827–2833

to insertion of the sample, the cartridge was filled with a blank sample (PBS or FBS) to allow imaging before virus accumulation occurs.

**Virus Creation, Preparation, and Use.** The recombinant vesicular stomatitis viruses which express the native Ebola glycoproteins were created by inserting the protein cDNA into an independent transcription start/stop sequence between the M and L genes in a VSV genome, where the VSV glycoprotein sequence had been removed.

## ASSOCIATED CONTENT

### Supporting Information

The Supporting Information is available free of charge on the ACS Publications website at DOI: 10.1021/acsnano.5b07948.

Further description of the particle detection software (PDF)

Movie demonstrating virus binding and single virus detection. The movie was created using the images acquired from the SP-IRIS sensor system with minimal postprocessing (AVI)

## AUTHOR INFORMATION


### Corresponding Author

*E-mail: selim@bu.edu.

### Author Contributions

#J.H.C. and M.S.U. share equal contribution as senior author.


### Notes

The authors declare no competing financial interest.

## ACKNOWLEDGMENTS

We thank M. Cabodi and E. Cevik for their support and help in experimental design, as well as E. Carter for conducting the plaque assay. This work was funded in part by the National Institutes of Health (R01AI1096159) and National Science Foundation (AIR-1127833).

## REFERENCES


(1) Mahy, B. *Microbiology and Microbial Infection*, 9th ed.; Hodder Arnold, 1998.

(2) Fumagalli, L.; Esteban-Ferrer, D.; Cuervo, A.; Carrascosa, J. L.; Gomila, G. Label-Free Identification of Single Dielectric Nanoparticles and Viruses with Ultraweak Polarization Forces. *Nat. Mater.* **2012**, *11*, 808−816.

(3) Brandenburg, B.; Zhuang, X. Virus Trafficking−learning from Single-Virus Tracking. *Nat. Rev. Microbiol.* **2007**, *5*, 197−208.

(4) Chan, W. M.; Bartee, E. C.; Moreb, J. S.; Dower, K.; Connor, J. H.; McFadden, G. Myxoma and Vaccinia Viruses Bind Differentially to Human Leukocytes. *J. Virol.* **2013**, *87*, 4445−4460.

(5) Jesus, D. M.; Moussatche, N.; McFadden, B. B. D.; Nielsen, C. P.; D'Costa, S. M.; Condit, R. C. Vaccinia Virus Protein A3 Is Required for the Production of Normal Immature Virions and for the Encapsidation of the Nucleocapsid Protein L4. *Virology* **2015**, *481*, 1−12.

(6) Kramberger, P.; Ciringer, M.; Štrancar, A.; Peterka, M. Evaluation of Nanoparticle Tracking Analysis for Total Virus Particle Determination. *Virol. J.* **2012**, *9*, 265.

(7) Gilmore, B. L.; Showalter, S. P.; Dukes, M. J.; Tanner, J. R.; Demmert, A. C.; McDonald, S. M.; Kelly, D. F. Visualizing Viral Assemblies in a Nanoscale Biosphere. *Lab Chip* **2013**, *13*, 216−219.

(8) Rossi, C.; Kearney, B.; Olschner, S.; Williams, P.; Robinson, C.; Heinrich, M.; Zovanyi, A.; Ingram, M.; Norwood, D.; Schoepp, R. Evaluation of ViroCyt® Virus Counter for Rapid Filovirus Quantitation. *Viruses* **2015**, *7*, 857−872.

(9) Garza-Licudine, E.; Deo, D.; Yu, S.; Uz-Zaman, A.; Dunbar, W. B. Portable Nanoparticle Quantization Using a Resizable Nanopore Instrument - The IZON qNanoTM. *IEEE Eng. Med. Biol. Soc.* **2010**, 5736−5739.

(10) Akpinar, F.; Yin, J. Characterization of Vesicular Stomatitis Virus Populations by Tunable Resistive Pulse Sensing. *J. Virol. Methods* **2015**, *218*, 71−76.

(11) Filipe, V.; Hawe, A.; Jiskoot, W. Critical Evaluation of Nanoparticle Tracking Analysis (NTA) by NanoSight for the Measurement of Nanoparticles and Protein Aggregates. *Pharm. Res.* **2010**, *27*, 796−810.

(12) Wang, S.; Shan, X.; Patel, U.; Huang, X.; Lu, J.; Li, J.; Tao, N. Label-Free Imaging, Detection, and Mass Measurement of Single Viruses by Surface Plasmon Resonance. *Proc. Natl. Acad. Sci. U. S. A.* **2010**, *107*, 16028−16032.

(13) Vollmer, F.; Arnold, S. Whispering-Gallery-Mode Biosensing: Label-Free Detection down to Single Molecules. *Nat. Methods* **2008**, *5*, 591−596.

(14) Zhuo, Y.; Hu, H.; Chen, W.; Lu, M.; Tian, L.; Yu, H.; Long, K. D.; Chow, E.; King, W. P.; Singamaneni, S.; Cunningham, B. T. Single Nanoparticle Detection Using Photonic Crystal Enhanced Microscopy. *Analyst* **2014**, *139*, 1007−1015.

(15) Ymeti, A.; Greve, J.; Lambeck, P. V.; Wink, T.; van Hövell; Beumer; Wijn, R. R.; Heideman, R. G.; Subramaniam, V.; Kanger, J. S. Fast, Ultrasensitive Virus Detection Using a Young Interferometer Sensor. *Nano Lett.* **2007**, *7*, 394−397.

(16) Mitra, A.; Ignatovich, F.; Novotny, L. Real-Time Optical Detection of Single Human and Bacterial Viruses Based on Dark-Field Interferometry. *Biosens. Bioelectron.* **2012**, *31*, 499−504.

(17) Daaboul, G. G.; Yurt, a.; Zhang, X.; Hwang, G. M.; Goldberg, B. B.; Ünlü, M. S. High-Throughput Detection and Sizing of Individual Low-Index Nanoparticles and Viruses for Pathogen Identification. *Nano Lett.* **2010**, *10*, 4727−4731.

(18) Reddington, A. P.; Trueb, J. T.; Freedman, D. S.; Tuysuzoglu, A.; Daaboul, G. G.; Lopez, C. a.; Karl, W. C.; Connor, J. H.; Fawcett, H.; Unlu, M. S. An Interferometric Reflectance Imaging Sensor for Point of Care Viral Diagnostics. *IEEE Trans. Biomed. Eng.* **2013**, *60*, 3276−3283.

(19) Cretich, M.; Pirri, G.; Damin, F.; Solinas, I.; Chiari, M. A New Polymeric Coating for Protein Microarrays. *Anal. Biochem.* **2004**, *332*, 67−74.

(20) Takada, a; Robison, C.; Goto, H.; Sanchez, a; Murti, K. G.; Whitt, M. a; Kawaoka, Y. A System for Functional Analysis of Ebola Virus Glycoprotein. *Proc. Natl. Acad. Sci. U. S. A.* **1997**, *94*, 14764−14769.

(21) Hack, H. R.; Wisniewski, M. L.; Josleyn, M. D.; Kwilas, S. A.; Van Deusen, N.; Mbaya, O. T.; Zhou, Y.; Stanley, D. a; Bliss, R. L.; Cebrik, D.; Smith, K. S.; Shi, M.; Ledgerwood, J. E.; Graham, B. S.; Sullivan, N. J.; Jagodzinski, L. L.; Peel, S. a; Alimonti, J. B.; Hooper, J. W.; Silvera, P. M.; et al. A Recombinant Vesicular Stomatitis Virus Ebola Vaccine — Preliminary Report. *N. Engl. J. Med.* **2015**, 1−10.

(22) Daaboul, G. G.; Lopez, C. a; Chinnala, J.; Goldberg, B. B.; Connor, J. H.; Unlü, M. S. Digital Sensing and Sizing of Vesicular Stomatitis Virus Pseudotypes in Complex Media: A Model for Ebola and Marburg Detection. *ACS Nano* **2014**, *8*, 6047.

(23) Lowe, D. G. Distinctive Image Features from Scale-Invariant Keypoints. *Int. J. Comput. Vis.* **2004**, *60*, 91−110.




DOI: 10.1021/acsnano.5b07948
*ACS Nano* 2016, 10, 2827−2833